Transport and Communications Science Journal, Special Issue (04/2025), 432-446

Transport and Communications Science Journal

EFFECTIVENESS STUDY ON THE WIND BARRIERS OF THE HSR BRIDGES IN WIND PRONE REGION

Guo Wei Wei [1], Xia Chao Yi [1], Bui Tien Thanh [2*]

[1] Beijing Jiaotong University, Beijing, China

[2*] University of Transport and Communications, No 3 Cau Giay Street, Hanoi, Vietnam

ARTICLE INFO

TYPE: Research Article
Received: 03/03/2025
Revised: 21/04/2025
Accepted: 28/04/2025
Published online: 30/04/2025
https://doi.org/10.47869/tcsj.76.2025.6
* *Corresponding author*
Email: btthanh@utc.edu.vn

Abstract. In areas frequently affected by strong winds, high-speed railway (HSR) bridges are commonly equipped with wind barriers to ensure train operational safety. This study focuses on a multi-span simply supported prestressed concrete bridge located along a real HSR line in Western China. Different barrier configurations with varying heights and porosities are investigated. A comprehensive wind-train-bridge interaction dynamic model is established to simulate the system's response, incorporating the effects of fluctuating crosswind velocities. Temporal histories of dynamic responses from both the train and the bridge are calculated and analyzed. A comparative evaluation of various barrier designs is conducted to determine their effectiveness in mitigating adverse wind effects. The results indicate that a barrier with a total height of 3.5 meters, consisting of 10% porosity in the lower 1.0 meter and 20% porosity in the upper 2.5 meters, provides the best performance in balancing wind shielding and structural stability. This research offers valuable insights for optimizing the design of wind barriers on HSR bridges in high-wind regions.

Keywords: High-speed railway, numerical simulation, simply-supported bridge, running safety, wind barrier.

@ 2025 University of Transport and Communications

1. INTRODUCTION

The operational safety of high-speed trains on these structures is the first priority for engineers when designing high-speed rail bridges worldwide [1,2]. The bridge under wind action may have considerable deformation and experience low frequency vibration, and its serviceability and even structural stability are directly affected. Strong wind excitations acting on trains can cause significant vibrations, potentially leading to overturning or derailment, posing a serious risk to both operational safety and passenger comfort [3,4]. In a train-bridge system, vibrations generated by vehicles are conveyed from the wheels to the bridge deck, thereby magnifying the bridge's dynamic response, which may further exacerbate the associated vibration effects [5,6,7].

It is widely recognized that wind barriers can effectively reduce aerodynamic forces on bridges, making them essential in HSR bridge design and construction in strong wind regions [8-9]. However, these barriers also introduce certain drawbacks, as they inevitably increase the windward surface area of the structure [10]. Moreover, their existence exacerbates turbulence effects, further complicating the wind field surrounding the bridge. As a result, the aerodynamic dynamics of the integrated train-bridge-barrier system have emerged as a significant area of research in recent decades.

Li, Zhou and Wang [11] performed wind tunnel tests and coupling vibration analyses to elucidate the impact of aerodynamic interference from wind barriers on the dynamic response of a long-span arch bridge system. Nuñez [12] investigated the function of wind barriers in alleviating aeroelastic instabilities in a cable-stayed bridge featuring a hinged-deck cross-section and assessed the implications of barrier porosity. Short-span bridges in areas with heavy winds should also be equipped with wind barriers, in addition to long-span bridges. Wang [13] employed a mobile model testing apparatus within a wind tunnel to investigate the dynamic interaction between wind barriers and the aerodynamic performance of a moving train. Zhang [14] investigated multiple solutions to alleviate the unstable crosswind effects on high-speed trains as they approach the end of windbreaks.

The windproof design of bridge barriers typically comprises two components. One involves structural selection informed by aerodynamic performance assessed by wind tunnel experiments and associated numerical techniques, while the other pertains to optimal selection based on the vehicle's operational safety metrics, utilizing coupled wind-train-bridge dynamic simulations. The author has analyzed the protective effect of a specific wind barrier [10], but further analysis is required on the scheme comparison of different barrier types. This study primarily examines the latter element, including natural winds, train vehicles, and an HSR just provided integrated support for a box girder bridge made of prestressed concrete (PC). A time-history simulation is performed to evaluate a train traversing a bridge amidst intense crosswinds, considering different wind speeds and barrier arrangements. The train's operational safety metrics and the bridge's dynamic responses are then calculated and contrasted. The numerical findings indicate the recommended design for the most effective wind barrier.

2. WIND-TRAIN-BRIDGE INTERACTION SYSTEM'S DYNAMIC ANALYSIS MODEL

The interaction system between wind, trains, and bridges demonstrates intricate, time-dependent dynamic behavior affected by numerous interconnected elements. Typically, this problem is addressed through transient analysis of an integrated spatial model that combines various sub-models.

- **Train model**

Generally, a high-speed train is composed of several powered and non-powered cars, commonly referred to as motor and trailer cars, respectively, as well as their suspension systems. In the simulation, each vehicle comprises a car body, four wheelsets, two bogies, and suspension systems linking the three components. After simplification, each car body has five degrees-of-freedom (DOFs), including the vertical floating Z_c, the lateral swing Y_c, the rolling θ_c, the yawing ψ_c and the pitching φ_c. Similarly, each bogie also has 5 DOFs of vertical floating Z_t, lateral swing Y_t, rolling θ_t, yawing ψ_t and pitching φ_t. To consider a tightly-contact wheel/rail interaction, only 3 DOFs of the vertical floating Z_w, the lateral swing Y_w and the rolling θ_w are assigned to each wheelset. Consequently, a vehicle model with 27 DOFs is developed for a four-axle train car, as illustrated in Fig. 1.

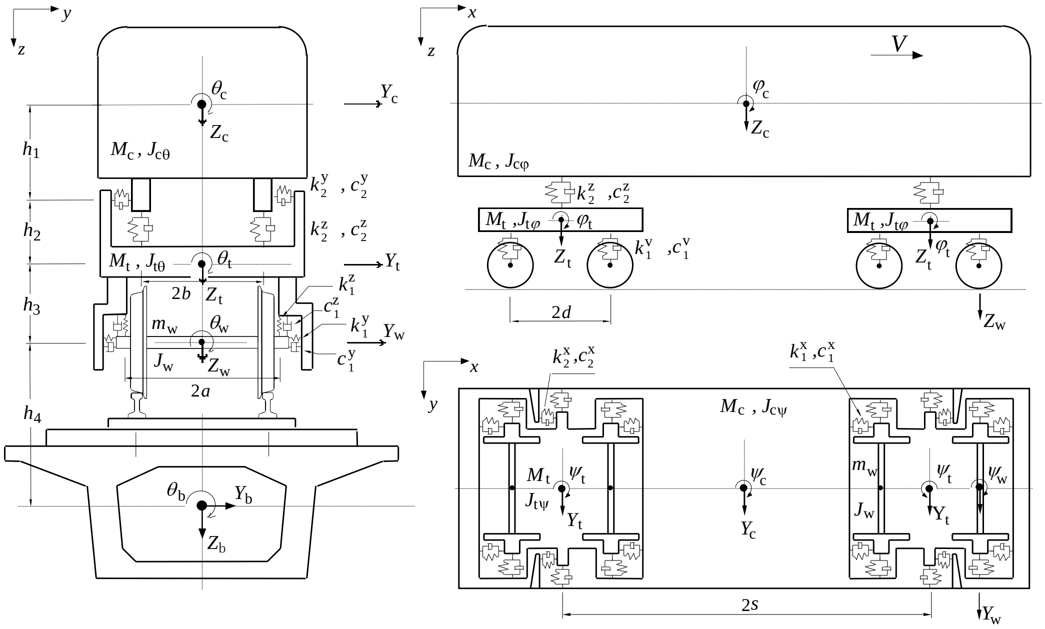

Figure 1. The vehicle model with 27 DOFs [15].

- **Bridge Model**

The bridge is modeled as a 3D finite element system composed of girders, deck system and tracks. It assumes that the track, ballastless slab and bridge deck have no relative displacement. By applying the modal comprehension analysis technique, the DOF number of the bridge could be significantly reduced [16]. The track is not modeled in this paper, and its dynamic coupling effect with the train and bridge models is considered by inputting the track irregularities into the train-bridge system. In the model, the wheel-rail force on each wheel-set transmit directly onto the bridge deck, and it is distributed to the two adjacent nodes. The distributed magnitude is inversely proportional to the force-to-node distance.

- **Wind Model**

The wind action may be divided into three components: x, y, and z, and it varies over the bridge deck. Consequently, the wind velocity field around the bridge structure is defined as a Gaussian stochastic process with multidimensional, multivariate, and homogeneous characteristics. For computational simplification, it is often regarded as three distinct, one-dimensional, multivariate random processes, neglecting inter-dimensional coherence. Assuming this, the wind velocity field during the simulation of a train traversing the bridge deck may be represented using multivariate stochastic processes in the y-z plane. Various numerical approaches can be employed to model stochastic wind velocity processes, including the spectrum representation method, the auto-regressive moving-average method, and the covariance decomposition method. In this research, a fast spectral representation technique is selected for modeling turbulent wind, utilizing an explicit formulation of Cholesky's decomposition based on the work of Cao, Xiang and Zhou [17]. Considering the specifications of a level bridge deck, evenly distributed wind velocity simulation locations, and a constant mean wind velocity along with its spectrum throughout the deck, the time histories of the along-wind (y-direction) component $u_i(t)$ and the upward wind (z-direction) component $w_i(t)$ at the ith simulation point (i=1,2,…,N) can be produced using the following equations:

$$\begin{cases} u_i(t) = \sqrt{2(\Delta\omega)}\sum_{m=1}^{i}\left[\sum_{k=1}^{N_\mathrm{f}}\sqrt{S_\mathrm{u}(\omega_{mk})}\times G_{im}(\omega_{mk})\times\cos(\omega_{mk}t+\varphi_{mk})\right] \\ w_i(t) = \sqrt{2(\Delta\omega)}\sum_{m=1}^{i}\left[\sum_{k=1}^{N_\mathrm{f}}\sqrt{S_\mathrm{w}(\omega_{mk})}\times G_{im}(\omega_{mk})\times\cos(\omega_{mk}t+\varphi_{mk})\right] \end{cases} \tag{1}$$

where, $S_\mathrm{u}(\omega_{mk})$ and $S_\mathrm{w}(\omega_{mk})$ are the spectral densities of along-wind and upward turbulent winds, respectively; N represents the total count of the simulation points; N_f is the total quantity of frequency interval $\Delta\omega$ in the frequency domain; φ_{mk} represents a random variable uniformly distributed throughout the range of 0 to 2π; $G_{im}(\omega_{mk})$ denotes the correlation matrix between the wind velocities at the points of i and m.

The aerodynamic forces acting on the bridge deck can be classified into three components: drag, lift, and moment. Each component consists of a static force generated by the mean wind, buffeting forces produced by turbulent wind, and self-exciting forces arising from the interplay between wind and bridge motion. By integrating quasi-steady aerodynamic force coefficients and neglecting the interaction between buffeting and self-exciting forces, the buffeting forces at the ith node of the bridge deck can be modeled [18].

The static wind force acting on a unit length of the bridge can be expressed as:

$$\begin{cases} F_\mathrm{BD}^\mathrm{st} = 0.5\rho U^2 C_\mathrm{BD}(\Psi)D \\ F_\mathrm{BL}^\mathrm{st} = 0.5\rho U^2 C_\mathrm{BL}(\Psi)B \\ F_\mathrm{BM}^\mathrm{st} = 0.5\rho U^2 C_\mathrm{BM}(\Psi)B^2 \end{cases} \tag{2}$$

where, $F_\mathrm{BD}^\mathrm{st}$, $F_\mathrm{BL}^\mathrm{st}$ and $F_\mathrm{BM}^\mathrm{st}$ are the buffeting lift, drag, and moment (the trio-components of the force F_B^st) on the bridge; ρ is the air density; U is the mean wind velocity; $C_\mathrm{BD}(\psi)$, $C_\mathrm{BL}(\psi)$ and $C_\mathrm{BM}(\psi)$ are the drag, lift, and moment coefficients under the wind attack angle ψ, and their reliable values are usually obtained using wind tunnel tests; D and B are the height and width of the girder, respectively.

The buffeting force acting on a unit length of the bridge is:

$$\begin{cases} F_\mathrm{BD}^\mathrm{bf} = 0.5\rho U^2 B\left[2\frac{D}{B}C_\mathrm{BD}(\Psi)\frac{u(x,t)}{U}\gamma_1(t)\right] \\ F_\mathrm{BL}^\mathrm{bf} = -0.5\rho U^2 B\left\{2C_\mathrm{BL}(\Psi)\frac{u(x,t)}{U}\gamma_2(t)+\left[C'_\mathrm{BL}(\Psi)+\frac{D}{B}C_\mathrm{BD}(\Psi)\right]\frac{w(x,t)}{U}\gamma_3(t)\right\} \\ F_\mathrm{BM}^\mathrm{bf} = 0.5\rho U^2 B^2\left[2C_\mathrm{BM}(\Psi)\frac{u(x,t)}{U}\gamma_4(t)+C'_\mathrm{BM}(\Psi)\frac{w(x,t)}{U}\gamma_5(t)\right] \end{cases} \tag{3}$$

where, F_{BL}^{bf}, F_{BD}^{bf} and F_{BM}^{bf} are the buffeting lift, drag, and moment (the trio-components of the force F_{B}^{bf}) on the bridge; C'_{BD} and C'_{BM} are the slopes of the lift, and moment coefficients; $\gamma_1 \sim \gamma_5$ are aerodynamic admittance functions in time domain. Comprehensive methodologies for computing buffeting force encompassing lift, drag, and moment at the *i*th node, are available in the author's prior publication [19].

The self-exciting forces on the bridge deck are depicted by convolution integrals, which connect bridge motion to impulse response functions. Due to the narrow carriage width (about 3m) and the blunted cross-section, its aerodynamic coupling effect with bridge is relatively weak. Therefore, the self-excited force is ignored in the wind-vehicle-bridge interaction analysis.

The wind area distribution around a high-speed train (HSR) vehicle is investigated and presented in Fig. 2 for different attack angles.

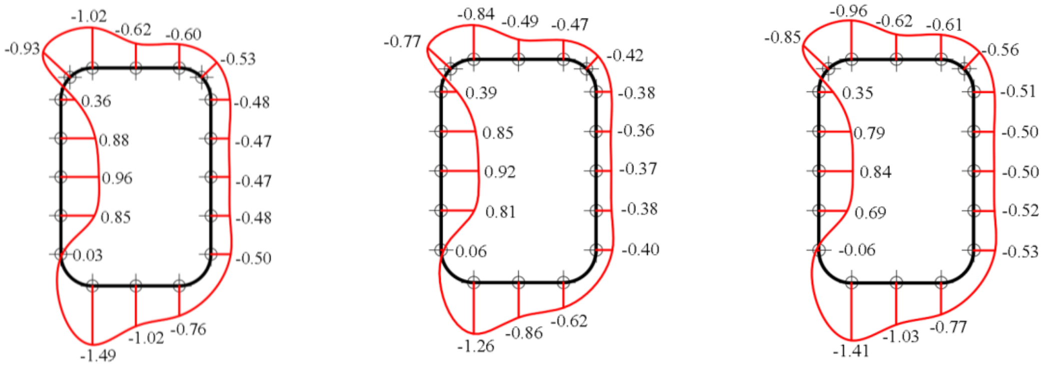

(a) -3° (b) 0° (c) +3°

Figure 2. Mean pressure coefficients of vehicle at different wind-attack angle.

Herein, the train model was located at the windward track. The oncoming flow speed was set as 12 m/s. A positive value of the pressure coefficient indicates that the force is directed towards the vehicle surface, while a negative value indicates the opposite direction. It is seen that the positive pressure coefficients distribute on the windward side of the vehicle surface with the maximum value of about 0.96. The negative values distribute on the top, bottom and leeward side of the vehicle. The minimum negative pressure coefficient appears at the windward corner of the vehicle bottom with the value of about 1.49.

Both static and buffeting wind forces acting on the vehicle are included, whereas self-exciting forces are disregarded for simplification [7]**.** In the bridge deck model, represented using 3D beam elements, the buffeting forces on the vehicles are obtained through interpolation between the buffeting forces at two adjacent nodes of the model. The static wind force is influenced solely by the mean component of the incoming wind. Consequently, the steady state drags, lift, and moment acting on the car body (the trio-components of the force F_{V}^{st}) at the mean wind velocity U can be expressed as:

$$\begin{cases} F_{vD}^{st} = 0.5\rho A V_R^2 C_{VD}(\Psi) \\ F_{vL}^{st} = 0.5\rho A V_R^2 C_{VL}(\Psi) \\ F_{vM}^{st} = 0.5\rho A V_R^2 H C_{VM}(\Psi) \end{cases} \tag{4}$$

where, $C_{VD}(\psi)$, $C_{VL}(\psi)$ and $C_{VM}(\psi)$ are the drag, lift, and moment coefficients of the vehicle under the wind attack angle ψ, and they are obtained by wind tunnel tests; A is the area at the windward side of car-body; V_R is the resultant velocity of mean wind velocity U and train speed V, which can be expressed as:

$$\begin{cases} V_R = \sqrt{U^2 + V^2} \\ \psi = \arctan(U/V) \end{cases} \tag{5}$$

The buffeting wind force F_V^{bf} on vehicle could be solved according to Equation (3), in which the pulsating wind velocities in the transverse and vertical directions are same as those of the bridge section where the vehicle runs.

- **Coupling dynamic equations of wind-train-bridge interaction system**

The wind-train-bridge system's dynamic equations may be expressed as follows by combining the train, bridge, and wind models [16]:

$$\begin{cases} M_V\ddot{\delta}_V + C_V\dot{\delta}_V + K_V\delta_V = F_V + F_V^{st} + F_V^{bf} \\ \ddot{q} + \Phi^T C_B \Phi \dot{q} + \Phi^T K_B \Phi q = \Phi^T\left(F_B + F_B^{st} + F_B^{bf}\right) \end{cases} \tag{6}$$

In this formulation, the subscripts V and B denote the vehicle and the bridge, respectively. The displacement vector of the vehicle is represented by δ_V, while M_V, C_V and K_V correspond to the mass, damping, and stiffness matrices of the vehicle. Similarly, q represents the displacement vector of the bridge in modal coordinates, and Φ is the mode shape matrix. The damping and stiffness matrices of the bridge are denoted as C_B and K_B, respectively. The force vectors F_V and F_B arise from interaction between the train and the bridge. The static and buffeting force vectors acting on the vehicle are denoted as F_V^{st} and F_V^{bf}, respectively, and they are applied onto the car-bodies of all analyzed vehicles simultaneously. Due to the relatively small magnitudes, the wind forces acting on the bogies and wheel-sets are ignored in calculation. For the bridge, the static and buffeting force vectors are represented as F_B^{st} and F_B^{bf}, respectively.

Equation (6) is a second-order linear non-homogeneous differential equation featuring time-dependent coefficients. The solution is obtained with the Newmark implicit integration method with specified parameters β = 0.25 and γ = 0.5. The integration time step is established at 0.002 seconds to guarantee enough computational precision. The train and bridge equations are solved at each iteration step, until reaching a convergency error when the force and moment differences are 10N and 10N·m comparing to those at previous step. Otherwise, the train and bridge vibration are not coupled sufficiently.

3. CASE STUDY OF WIND-TRAIN-BRIDGE INTERATION CONSIDERING DIFFERENT WIND BARRIERS

A genuine high-speed rail project in northwest China, situated in a windy area susceptible to strong windstorms, has been chosen as the case study. At the bridge location, the average wind velocity surpasses 20 m/s and last for almost 4 hours daily, although instantaneous wind velocities may attain 40–50 m/s. Under these circumstances, assessing the efficacy of windbreaks is essential for guaranteeing the operational safety of high-speed trains traversing the area.

- **Description of bridge and barrier structures**

The multi-span simply supported PC box girder bridge with 32 m span is most widely used in the windy zones in China. The box section has a width of 13.4 meters and a height of 3.05 meters. As an illustrative case study, this paper takes a 10-span bridge to perform the dynamic analysis. The single-column piers with a height of 15 m are selected, and the average elevation of the deck is 18.05 m.

The wind barrier schemes in this paper include the unilateral and the bilateral structures, the straight and curved structures, with different heights, as shown in Fig. 3.

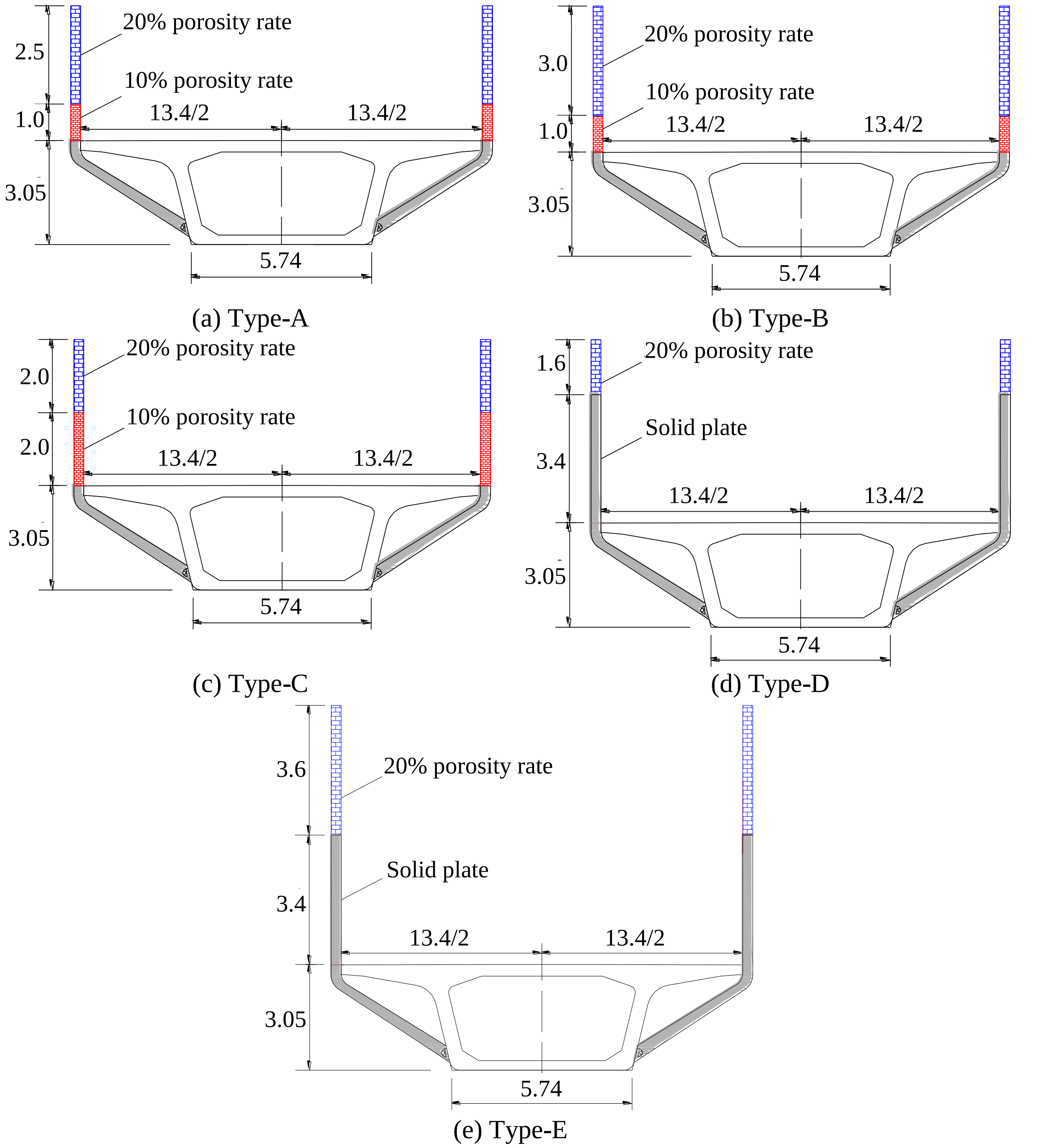

Figure 3. Wind barriers designed for the bridges in windy zone (unit: m).

The barrier structures studied in this paper are all composed of columns and screens. The columns, made of hot-rolled H-shaped steel, are embedded within the beam, while 4 mm thick screens are attached to these columns. All components are secured using bolted connections. In the numerical model, the screens are fixed rigidly on the bridge. The configuration details could be found in authors' previous study [10].

Detailed information is available in Table 1.

Table 1. Features of the wind barriers

Type	Description
A	height of 3.5 m, 10% porosity at the bottom 1.0 m and 20% porosity at the above 2.5 m
B	height of 4.0 m, 10% porosity at the bottom 1.0 m and 20% porosity at the above 3.0 m
C	height of 4.0 m, 10% porosity at the bottom 2.0 m and 20% porosity at the above 2.0 m
D	height of 5.0 m, 0% porosity at the bottom 3.4 m and 20% porosity at the above 1.6 m
E	height of 7.0 m, 0% porosity at the bottom 3.4 m and 20% porosity at the above 3.6 m

The bridge model, including beams, piers and their connections is established by the MIDAS software. The pier bottom is fixed rigidly, and the beam ends are constrained onto the pier-top with either fixed or movable bearing connection. Since the barriers have much smaller stiffness compared with the bridge, and their structures are not incorporated into the FE model (see Fig. 4).

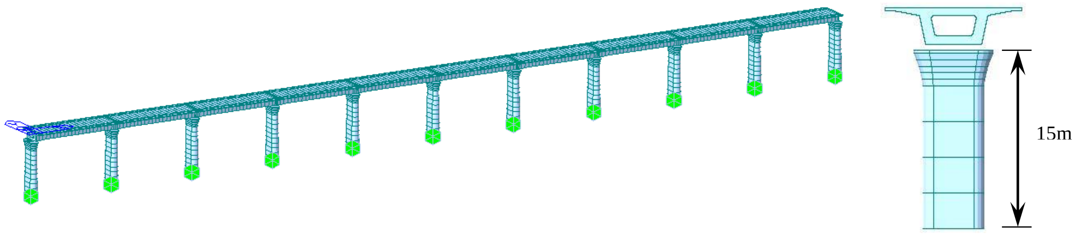

(a) Overall view (b) Sectional view

Figure 4. The 3D FE bridge model.

The dynamic features of the bridge, encompassing its inherent frequencies and mode shapes, are ascertained by eigenvalue analysis. Some of the mode shapes are shown in Fig. 5.

(a) 1st lateral bending mode (b) 2nd lateral bending mode (c) 3rd lateral bending mode

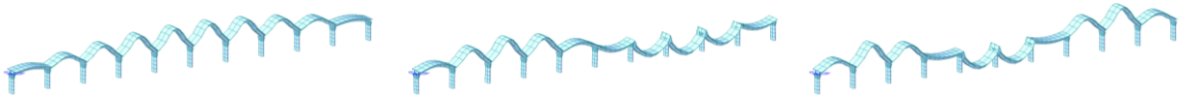

(d) 1st vertical bending mode (e) 2nd vertical bending mode (f) 3rd vertical bending mode

Figure 5. The mode shapes of the 10×32m HSR bridge.

The frequencies for the fundamental lateral and vertical vibration modes are 3.274 Hz and 4.154 Hz, respectively. The first 80 modes, up to a natural frequency of 31.887 Hz, are considered for mode superposition. Since no measured data is available for the new HSR bridges, a homogeneous damping ratio of 2.5% is assumed for all modes in reference of the measurement and simulation from two similar HSR simply-supported bridges [20-21].

- **Description of High-speed Train**

In this study, a high-speed EMU train with a configuration of 4×(3M+1T) is modeled, where M and T represent the motorcar and trailer car, respectively. The overall dimensions of each car are 24.775 m in length, 2.7 m in width, and 3.5 m in height, as illustrated in Fig. 6.

Figure 6. Configuration of high-speed train (unit: cm) [16].

- **Description of Track Irregularities**

The irregularity spectra $S(f)$ (unit: $mm^2/(1/m)$) of the ballasted track in China is adopted, to generate stochastic samples of track irregularities in various directions [22].

$$S(f)=\frac{A(f^2+Bf^3+C)}{f^4+Df^3+Ef^2+Ff+G} \tag{7}$$

Here, f denotes the spatial frequency associated with track irregularities (1/m); The parameters of A, B, C, D, E, F and G are listed in Table 2.

Table 2. Parameters of the track irregular spectra.

Irregularity Type	**Fitted Parameters**						
	A	*B*	*C*	*D*	*E*	*F*	*G*
Left vertical	1.1029	-1.4709	0.5941	0.8480	3.8016	-0.2500	0.0112
Right vertical	0.8581	-1.4607	0.5848	0.0407	2.8428	-0.1989	0.0094
Left lateral	0.2244	-1.5746	0.6683	-2.1466	1.7665	-0.1506	0.0052
Right lateral	0.3743	-1.5894	0.7265	0.4353	0.9101	-0.0270	0.0031
Torsional	0.1214	-2.1603	2.0214	4.5089	2.2227	-0.0396	0.0073

Track irregularities over a 2,600 m section, encompassing deviations to the left, right, left lateral, and left vertical for both rails, are simulated. The corresponding maximum and minimum values are provided in Table 3.

Table 3. Amplitudes of the track irregularities (unit: mm).

Vertical		**Lateral**	
Left	Right	Left	Right
4.89	4.61	5.06	5.50

- **Description to Wind forces on the Coupling System**

The stochastic wind velocity field is generated by Equation (1), in which the auto-spectra of along wind and upward winds are selected according to the Chinese Code [23].

$$\begin{cases} S_u(\omega)=\dfrac{2\pi}{\omega}\cdot\dfrac{200f(z)u_*^2}{\left[1+50f(z)\right]^{5/3}} \\ S_w(\omega)=\dfrac{2\pi}{\omega}\cdot\dfrac{6f(z)u_*^2}{\left[1+4f(z)\right]^2} \end{cases} \tag{8}$$

$$f(z)=\frac{\omega z}{2\pi U_z} \tag{9}$$

$$u_*=\frac{0.4U_z}{\ln\dfrac{Z-H+2.5Z_0}{Z_0}} \tag{10}$$

where U_z signifies the mean wind velocity along the primary wind direction at height z; u_* indicates the frictional wind velocity; H represents the average height of the adjacent structures; Z_0 corresponds to the ground roughness length.

The coherence function adheres to Davenport's formulation:

$$\mathrm{Coh}_{ij}(\omega)=\exp(-\lambda_{ij}\cdot\frac{\omega_{ij}}{2\pi U_z}) \tag{11}$$

where, r_{ij} is the distance between the points i and j; λ is the correlation coefficient, ranging from 7 to 12.

A total of 201 simulation points is evenly distributed along the bridge deck, with a separation of 5.0 m. The sampling frequency and frequency interval for turbulent wind velocity in the simulation are established at 50 Hz and 0.001 Hz, respectively. The overall simulation duration is 10 minutes, with a time interval of 0.02 seconds.

Using the drag, lift, and moment coefficients of the train-bridge-barrier system ascertained through actual wind tunnel experiments [24], the influence of the wind barriers is considered in this study instead of modeling a fine bridge with barrier. Tables 4 and 5 present the drag, lift, and moment coefficients, along with their first derivatives at a zero angle of attack for the coupling system.

Table 4. Tri-component coefficients and derivatives of deck.

Barrier Type	**Deck**					
	C_{BD}	C_{BL}	C_{BM}	C'_{BD}	C'_{BL}	C'_{BM}
No Barrier	2.109	-0.202	-0.015	0.349	-2.009	0.105
A	3.503	0.055	0.371	2.474	0.280	0.518
B	3.639	0.103	0.267	3.596	-0.119	0.562
C	3.684	-0.027	0.335	3.040	-0.261	0.495
D	3.924	-0.051	0.255	2.363	-1.344	0.174
E	4.896	-0.302	0.341	1.012	-0.007	0.232

Table 5. Tri-component coefficients and derivatives of vehicle.

Barrier Type	**Vehicle**					
	C_{VD}	C_{VL}	C_{VM}	C'_{VD}	C'_{VL}	C'_{VM}
No Barrier	1.911	-0.001	0.943	-0.369	6.509	0.426
A	0.161	0.022	0.144	-0.751	-0.383	-0.616
B	0.219	-0.002	0.109	-0.483	0.050	-0.487
C	0.177	0.021	0.099	-0.676	-0.181	-0.598
D	0.096	0.084	0.066	0.551	0.086	-0.430
E	0.075	0.102	0.077	-0.078	1.113	-0.073

Based on the generated stochastic wind velocities as well as the tri-component coefficients above, the wind forces acting on the bridge and vehicle could be obtained using the equations in Chapter 2.

4. EFFECTIVENESS ANALYSIS OF WIND BARRIERS BASED ON NUMERICAL RESULTS

- **Numerical Simulation of Wind Velocities and Forces**

For an instantaneous wind velocity of 30 m/s, accompanied by a mean wind velocity of approximately 22 m/s, the time histories of lateral and vertical wind velocities at the bridge deck are simulated, as depicted in Fig. 7.

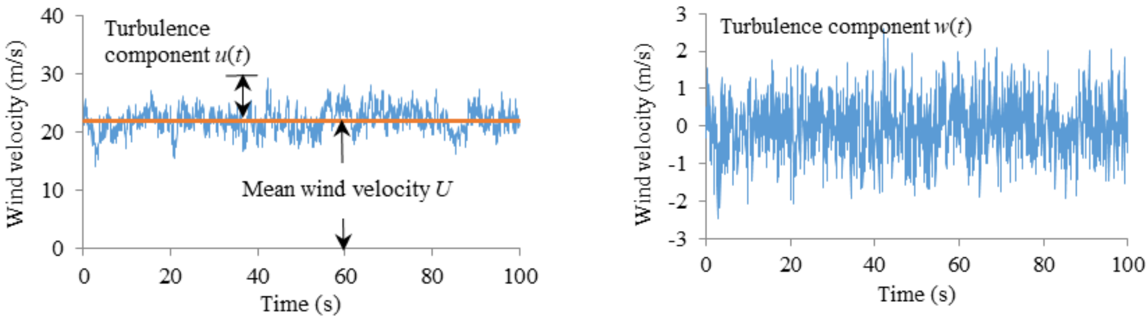

(a) Lateral (b) Vertical

Figure 7. Simulated instantaneous, mean and turbulence wind at the bridge deck.

Fig. 8 presents the temporal histories of the initial modal buffeting drag and lift forces exerted on the bridge equipped with the Type-A barrier.

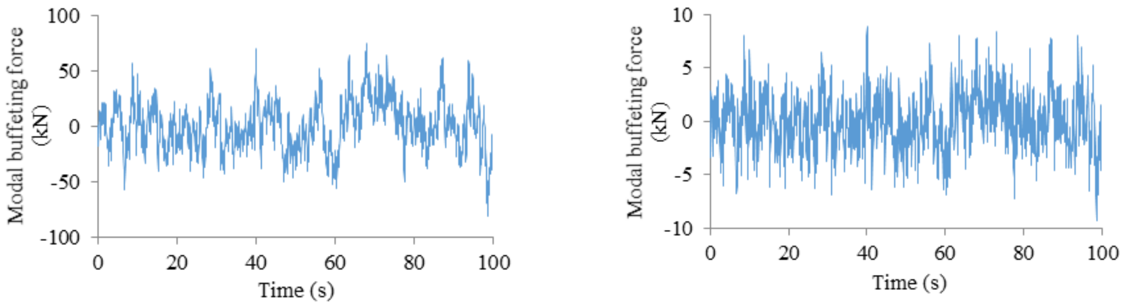

(a) Drag force (b) Lift force

Figure 8. Temporal data of first modal buffeting forces for the Type-A barrier case.

- **Dynamic Responses of Vehicles**

For a train running at 250 km/h on the bridge equipped with the Type-A barrier, the instantaneous wind velocity is 30 m/s, the time histories of the accelerations of the first motorcar are depicted in Fig. 9.

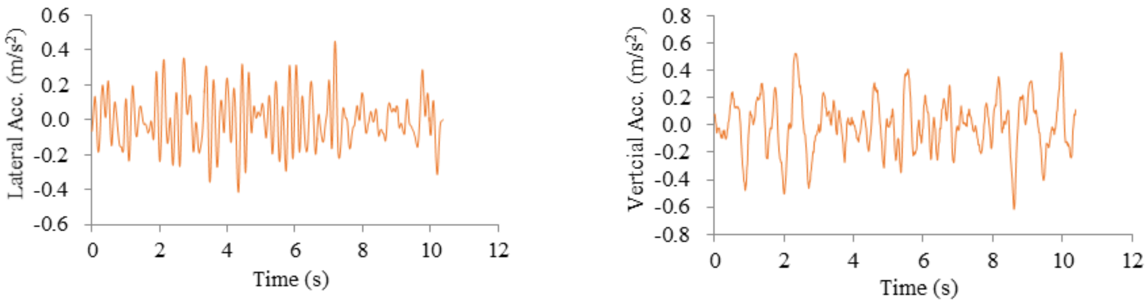

(a) Lateral (b) Vertical

Figure 9. Time histories of the accelerations of the first vehicle (The Type-A barrier).

The results show that the maximum vertical and lateral accelerations are 0.451 m/s^2 and 0.618 m/s^2, which appears at the last trailer car on the bridge with the Type-A barrier. However, the acceleration amplitudes at all analytical cases are not significantly different, and they are far lower than the allowable values of 1.0 m/s^2 and 1.3 m/s^2 in design code [25].

In China, the assessment of train running safety under strong crosswinds is based on the following evaluation indices: the derailment factor Q_w/P_w (defined as the ratio of the lateral force Q_w acting on the wheel-set to the total vertical force P_w acting on the same wheel-set at the climbing-up-rail side), the offload factor $\Delta P_w/P_w$ (defined as the ratio of the static and dynamic vertical force difference ΔP_w to the total vertical force P_w acting on the wheel-set), the lateral wheel force Q_w, and the overturn factor D_w (defined as the ratio of the overturn moment M_w to the anti-overturn moment of the vehicle aP_w, which is induced by the direct wind actions on the car-body). The allowable values of these indices in the Chinese code are as follows [25]:

Derailment factor: $$Q_w / P_w \le 0.8 \tag{12-a}$$

Offload factor: $$\Delta P_w / P_w \le 0.6 \tag{12-b}$$

Lateral wheel force: $$Q_w \le 10 + P_{w0} / 3 \tag{12-c}$$

Overturn factor: $$D_w = M_w / aP_w \le 0.8 \tag{12-d}$$

where, P_{w0} denotes the axial load (160 kN for the motorcar and 146 kN for the trailer car). The permissible lateral wheel forces in this study are 63.3 kN for the motorcar and 58.7 kN for the trailer car, respectively; a is half of the axle track.

The lateral and vertical forces as well as the moment on a wheel-set could be obtained by following equations:

$$Q_{\mathrm{w}} = -m_{\mathrm{w}}\ddot{Y}_{\mathrm{w}}^{2} + c_1^{y}(\dot{Y}_{\mathrm{t}} - h_3\dot{\theta}_{\mathrm{t}} + \eta d\dot{\psi}_{\mathrm{t}} - \dot{Y}_{\mathrm{w}}) + k_1^{y}(Y_{\mathrm{t}} - h_3\theta_{\mathrm{t}} + \eta d\psi_{\mathrm{t}} - Y_{\mathrm{w}}) \tag{13-a}$$

$$P_{\mathrm{w}} = -m_{\mathrm{w}}\ddot{Z}_{\mathrm{w}}^{2} + c_1^{z}(\dot{Z}_{\mathrm{t}} + \eta d\dot{\varphi}_{\mathrm{t}} - \dot{Z}_{\mathrm{w}}) + k_1^{z}(Z_{\mathrm{t}} + \eta d\varphi_{\mathrm{t}} - Z_{\mathrm{w}}) + g\left(m_{\mathrm{w}} + 0.5M_{\mathrm{t}} + 0.25M_{\mathrm{c}}\right) \tag{13-b}$$

$$M_{\mathrm{w}} = -J_{\mathrm{w}}\ddot{\theta}_{\mathrm{w}} + a^2c_1^{z}(\dot{\theta}_{\mathrm{t}} - \dot{\theta}_{\mathrm{w}}) + a^2k_1^{z}(\theta_{\mathrm{t}} - \theta_{\mathrm{w}}) + h_4Q_{\mathrm{w}} + eP_{\mathrm{w}} \tag{13-c}$$

where, J_{w} denotes the mass moment of inertia of wheel-set; e is the distance between the centerlines of track and bridge.

The train operates at a speed of 250 km/h, while the instantaneous wind velocity at the bridge site varies from 0 m/s to 40 m/s. The relevant running safety indices of the train are calculated and depicted in Fig. 10.

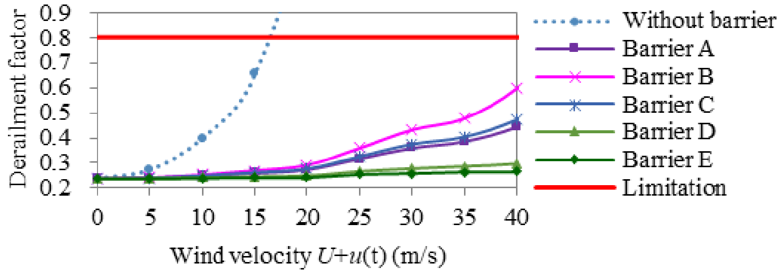

(a) Derailment factor

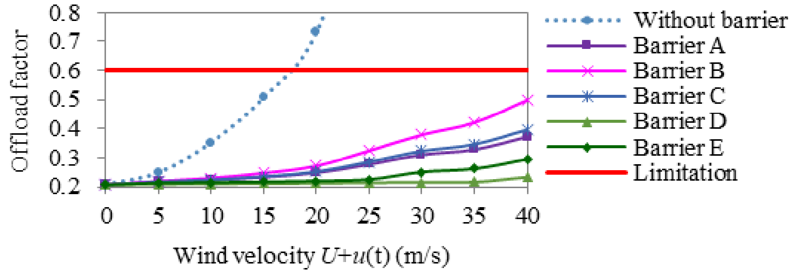

(b) Offload factor

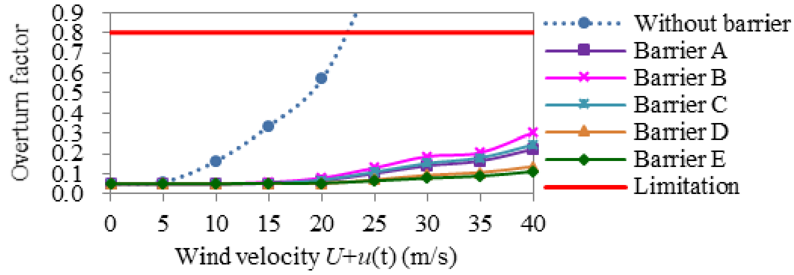

(c) Overturn factor

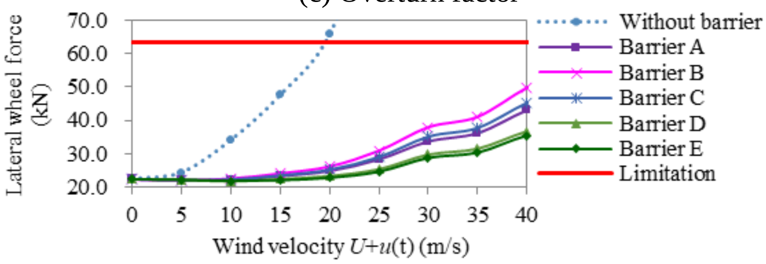

(d) Lateral wheel force of the motor-cars

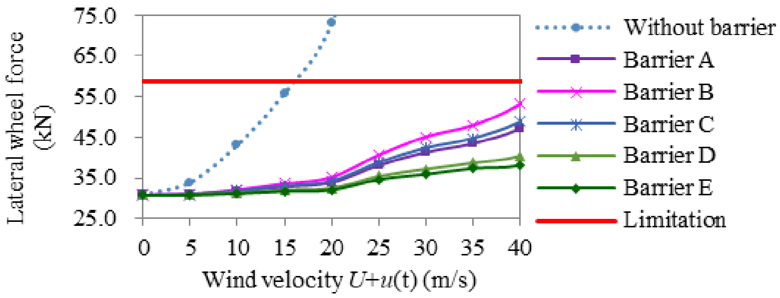

(e) Lateral wheel force of the trailer-cars

Figure 10. Correlation between the vehicle's highest lateral response and wind velocity

The findings demonstrate that all computed running safety indices rise with wind velocity. If there is no wind barrier, the indices will exceed the allowance in many cases, and the wind action may threaten the train's running safety at a low speed of 15 m/s. When the barriers are installed, the distribution curves grow more slowly. The comparison demonstrates that the wind barriers possess a distinct windbreak effect and improve the safety of train operations. In general, The Type-D and Type-E barriers show better performances at all cases, the others have sufficient redundancy to ensure the running-safety effectively.

- **Dynamic Responses of Bridge**

Illustrated in Fig. 11 is the time-histories of vertical displacement of the bridge deck at the 5th mid-span (displayed in the figures), when the train speed is 250 km/h and the instantaneous wind velocity is 30 m/s.

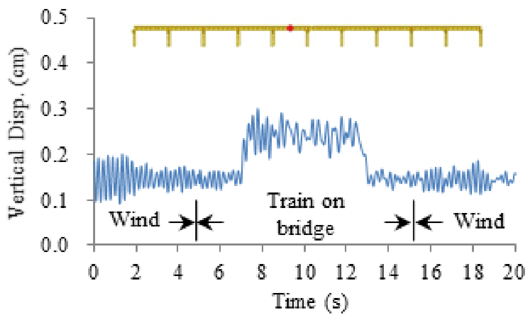

Figure 11. Time-histories of vertical displacement of the bridge deck (Type-A barrier).

Displayed in Fig. 12 is, respectively, the distributions of lateral displacement and acceleration of the bridge (y-direction) versus the wind velocity.

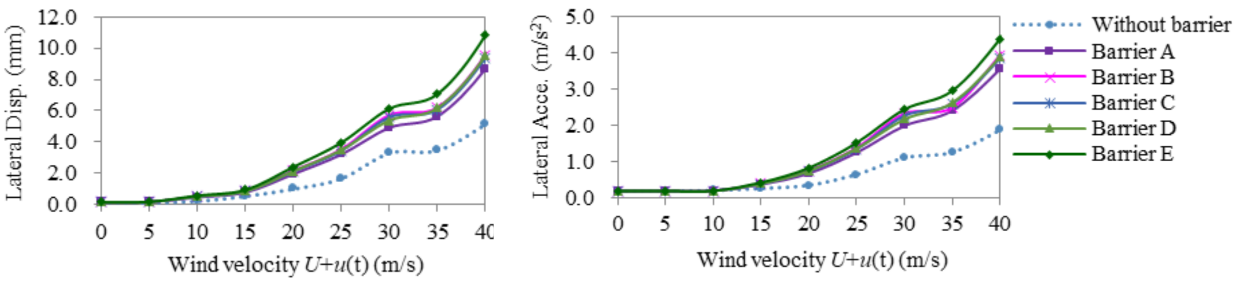

(a) Lateral displacement (b) Lateral acceleration

Figure 12. The maximum lateral responses of the bridge vs. wind velocity.

The substantial rise in bridge displacement and acceleration after the setting up of the wind barrier offers a challenge that necessitates consideration in structural design. Consequently, in determining and optimizing the wind barrier on high-speed rail bridges, it is essential to consider not merely the safety indices of trains but also the bridge's response as an important consideration. Figure 12 shows the Type-A causes the lowest bridge vibration except for no-barrier case.

A comprehensive analysis of the dynamic response of the train-bridge system as well as the construction cost indicates that, among the five previously mentioned types of bilateral straight steel barrier structures, the Type-A wind barrier shows the guarantee effectiveness in running safety, the optimal performance in bridge vibration and the least consumption in building material.

5. CONCLUSIONS

In this study, numerical simulations are conducted to analyze a high-speed train traversing a multi-span simply supported bridge under crosswind conditions. By comparing the dynamic responses of the coupled wind-train-bridge system, the effectiveness of various wind barrier designs is evaluated. From the results, the subsequent conclusions can be inferred:

- The wind velocity highly influences the train's running safety. If there has no wind barrier, all running safety indices are remarkably greater than the cases with the design barriers. Protected by the barrier structures, the train can still run safely on the bridge at the speed of 250 km/h even if the wind velocity reaches 40 m/s.

- Although beneficial for enhancing train safety, the protective design adversely affects the bridge. The installation of wind barriers markedly enhances both the lateral movement and accelerating of the bridge.

- Comparing the responses of both the vehicle and the bridge comprehensively, the bilateral straight steel barrier with the design parameters of 3.5 m height, 10% porosity in the lower 1.0 m, and 20% porosity in the upper 2.5 m is recommended. (Reviewer B, Q7)

It should be emphasized that: considering the simply supported bridge in this paper is obviously insufficient, especially for the selection and optimization of the wind barriers on HSR bridges in the windy zone. Therefore, further field measurement and numerical studies should be conducted, to explore more precise wind model reflecting different cases, more applicable wind-barriers for different bridge types, and more simpler methods in running safety evaluation.

ACKNOWLEDGMENT

The research is financially supported by the National Natural Science Foundations of China (Grant No. 51878036).

REFERENCES

[1]. X. H. He, Recent developments in the wind resistance of railway bridges in China, Advances in Wind Engineering, 1 (2024) 100027. https://doi.org/10.1016/j.awe.2024.100027

[2]. J. F. Mao, A Novel Hybrid Approach Combining PDEM and Bayesian Optimization Deep Learning for Stochastic Vibration Analysis in Train-Track-Bridge Coupled System, Reliability Engineering and System Safety, 257 (2025) 110827. https://doi.org/10.1016/j.ress.2025.110827

[3]. R. K. Cooper, The effect of cross winds on trains, Journal of Fluids Engineering, 103 (1981) 170-178. https://doi.org/10.1115/1.3240768

[4]. H. Hassan, Contribution of computational wind engineering in train aerodynamics—past and future. Journal of Wind Engineering and Industrial Aerodynamics, 234 (2023) 105352. https://doi.org/10.1016/j.jweia.2023.105352

[5]. Y. L. Li, Dynamics of wind-rail vehicle-bridge systems, Journal of Wind Engineering and

Industrial Aerodynamics, 93 (2005) 483-507. https://doi.org/10.1016/j.jweia.2005.04.001

[6]. Z. W. Xu, G. L. Dai, Y. F. Chen, H. M. Rao, Z. B. Huang, Extreme response analysis of train-track-bridge-wind interaction system based on in-situ monitoring wind data, Structural Safety, 100 (2023) 102288. https://doi.org/10.1016/j.strusafe.2022.102288

[7]. Y. L. Xu, N. Zhang, H. Xia, Vibration of coupled train and cable-stayed bridge system in cross wind", Engineering Structure, 26 (2004) 1389-1406. https://doi.org/10.1016/j.engstruct.2004.05.005

[8]. T. Fujii, T. Maeda, H. Ishida, T. Imai, K. Tanemoto, M. Suzuki, Wind-induced accidents of train/vehicles and their measures in Japan, Quarterly Report of RTRI, 40 (1999) 50-55.

[9]. B. D. Xiong, Sustainable wind barrier: Self-powered system for high-speed railway safety monitoring, Sustainable Materials and Technologies, 39 (2024) e00848.

[10].W. W. Guo, H. Xia, R. Karoumi, T. Zhang, X. Z. Li, Aerodynamic effect of wind barriers and running safety of trains on high-speed railway bridges under cross winds, Wind and Structures, 20 (2015) 213-236. https://doi.org/10.12989/was.2015.20.2.213

[11].X. Z. Li, Y. X. Zhou, M. Wang, Aerodynamic Interference and Dynamic Influence of Wind Barrier on Train-bridge Coupling Vibration, KSCE Journal of Civil Engineering System, 21 (2023) 3036-3047. https://doi.org/10.1007/s12205-023-1884-0

[12].E. Lopez-Nuñez, Effect of wind barriers on the aeroelastic instabilities of a hinged-deck cross-section cable-stayed bridge, Engineering Structures, 287 (2023) 116112, https://doi.org/10.1016/j.engstruct.2023.116112

[13].M. Wang, Z. X. Wang, X. W. Qiu, X. X. Li, X. Z. Li, Windproof performance of wind barrier on the aerodynamic characteristics of high-speed train running on a simple supported bridge, Journal of Wind Engineering and Industrial Aerodynamics, 223 (2022) 104950. https://doi.org/10.1016/j.jweia.2022.104950

[14].D. Q. Zhang, H. X. Gao, W. J. Jiang, X. H. Dong, J. Song, G. Hu, Mitigating crosswind response of a high-speed train passing the end of windbreak walls, Advances in Wind Engineering, 1 (2024) 100009. https://doi.org/10.1016/j.awe.2024.100009

[15].H. Xia, Y.L. Xu, T. H. T. Chan, Dynamic interaction of long suspension bridges with running trains, Journal of Sound and Vibration, 237 (2000) 263-280. https://doi.org/10.1006/jsvi.2000.3027

[16].H. Xia, D. R. Guido, J. M. Goicolea, Bridge Vibration and Controls: New Research, Nova Science Publishers, New York, 2012.

[17].Y. H. Cao, H. F. Xiang Haifan, Y. Zhou, Simulation of stochastic wind velocity field on long-span bridges, Journal of Engineering Mechanics, 126 (2000) 1-6, https://doi.org/10.1061/(ASCE)0733-9399(2000)126:1(1)

[18].E. Simiu, R. H. Scanlan Robert, Wind Effects on Structures: Fundamentals and Applications to Design, Wiley Publishing, New York, 1996.

[19].W. W. Guo, H. Xia, Y. L. Xu, Running safety analysis of a train on the Tsing Ma bridge under turbulent winds, Earthquake Engineering and Engineering Vibration, 9 (2010) 307-318. https://doi.org/10.1007/s11803-010-0015-3

[20].K. Liu, E.Reynders, G. De Roeck, G. Lombaert, Experimental and numerical analysis of a composite bridge for high-speed trains, Journal of Sound Vibration, 320 (2009) 201-220.

[21].P. Lou, A vehicle-track-bridge interaction element considering vehicle's pitching effect, Finite Elements in Analysis and Design, 4 (2005) 397-427.

[22].M. X. Chen, L. Wang, X. X. Tao, G. H. Cui, X. S. Chai, F. C. Yang, W. Q. Wu. Fitting method of track spectrum for main line railway in China (in Chinese), Journal of Traffic and Transportation Engineering, 8 (2008) 19-22. https://doi.org/10.3321/j.issn:1671-1637.2008.01.005

[23].MINISTRY OF TRANSPORT OF P. R. C., Wind-resistant Design Specification for Highway Bridges (JTGT3360-01-2018), People's Communications Publishing House Co., Ltd, Beijing (in Chinese), Mar. 2019.

[24].W. W. Guo, Y. J. Wang, H. Xia, S. Lu, Wind tunnel test on aerodynamic effect of wind barriers on train-bridge system, Science China Technological Sciences, 58 (2015) 219-225.

[25].NATIONAL RAILWAY ADMINISTRATION OF P. R. C., Code for design of high-speed railway (TB 10621-2014), China Railway Publishing House, Beijing (in Chinese), Dec. 2014.